INTERNATIONAL JOURNAL FOR NUMERICAL METHODS IN FLUIDS, VOL. 11, 361–377 (1990)

COMPUTING AXISYMMETRIC, LAMINAR INTERNAL FLOWS

R. W. DERKSEN

Department of Applied Mathematics, University of Western Ontario, London, Ontario, Canada N6H 4R5

SUMMARY

A simple computational scheme is developed to compute laminar flows inside axisymmetric ducts. It is based on the Keller box method where the equations are approximated at the centre of the downstream face of each computational box. The coupling between the pressure gradient and the velocities for internal flow has been observed to introduce stability problems for the Keller box method that are not present for external, boundary layer flow problems. The difference scheme for the velocities is coupled to an iterative scheme to solve for the pressure gradient at each axial step. Example results for developing flow in a pipe and in a 2° conical diffuser are presented.

KEY WORDS Internal flows Box methods

1. INTRODUCTION

Internal axisymmetric flows are regularly found in engineering applications, where typical examples are contraction sections, pipes and diffusers. It is desirable to be able to predict the flow properties such as the pressure drop and skin friction because of the widespread application of these devices. The equations of motion have yielded analytic solutions to only a few very special, simplified internal flows, where the classic example is the fully developed laminar flow in a pipe. However, most flows of interest are not amenable to analysis and one must resort to numerical approximation.

The demands on any numerical approximation scheme are very stringent: it must be accurate, it must be stable and it must perform under the constraints of the available computational resources of time and memory. Accurate solutions to both the cross-stream velocity distribution and the streamwise evolution of the velocities and the pressure gradients are required for non-self-similar flows.

Only incompressible laminar flows will be considered in this paper. Additionally, it will be assumed that the radius of the duct varies slowly in the streamwise direction. Liquids can be treated as incompressible in almost all cases and for low Mach numbers gases are also nearly incompressible, so the assumption of incompressible flows is not very restrictive. However, the assumption that the radius is varying slowly is more restrictive. It has been made to allow the use of the thin shear layer approximations to the equations of flow. For diverging ducts this assumption avoids the problem of separation with the attendant flow reversal. The FLARE approximation[1] can be used to deal with separation, and this will be employed in future developments of this method. Laminar flow has been assumed because the performance of any of the turbulence closure models is suspect except for the specific flows that they have been calibrated for.

0271–2091/90/120361–17$08.50

Received 30 June 1989
Revised 8 November 1989

A scheme was developed that was based on the Keller box finite difference method. It is different in that all of the equations are centred on the downstream face of the box. An iterative method is used to compute the pressure gradient for each axial step. Computational results from the scheme developed in this paper will be presented for two flows: developing flow in a circular pipe and flow in a 2° conical diffuser.

2. COMPUTATIONAL MODEL

The basic equations, in cylindrical co-ordinates, that govern the flow under these assumptions are the continuity equation

$$\frac{\partial U}{\partial \xi}+\frac{\eta f'(\xi)}{f(\xi)}\frac{\partial U}{\partial \eta}+\frac{f(\xi)}{\eta}\frac{\partial \eta V}{\partial \eta}=0 \tag{1}$$

and the momentum equation for the axial velocity component

$$U\left(\frac{\partial U}{\partial \xi}+\frac{\eta f'(\xi)}{f(\xi)}\frac{\partial U}{\partial \eta}\right)+Vf(\xi)\frac{\partial U}{\partial \eta}=-\frac{1}{\rho}\frac{dP}{d\xi}+\frac{f^2(\xi)}{\eta}\frac{\partial}{\partial \eta}\left(\eta\nu\frac{\partial U}{\partial \eta}\right). \tag{2}$$

Note that the (x,r) co-ordinate system has been transformed using the following relations:

$$\xi = x, \qquad \eta = rf(x). \tag{3}$$

This transformation allows a rectangular grid to be used in the computational domain if the function $f(x)$ normalizes the radius to range from zero to one at all axial locations.

The computational method is based on the Keller box scheme,[2-6] where the second-order system of partial differential equations is recast as a system of first-order partial differential equations. The Keller box method was originally developed for the thin shear layer equations of heat, momentum and scalar transport. Briefly, the second-order partial differential equations are converted to a system of first-order equations. This is done by setting

$$W = \partial U/\partial \eta \tag{4}$$

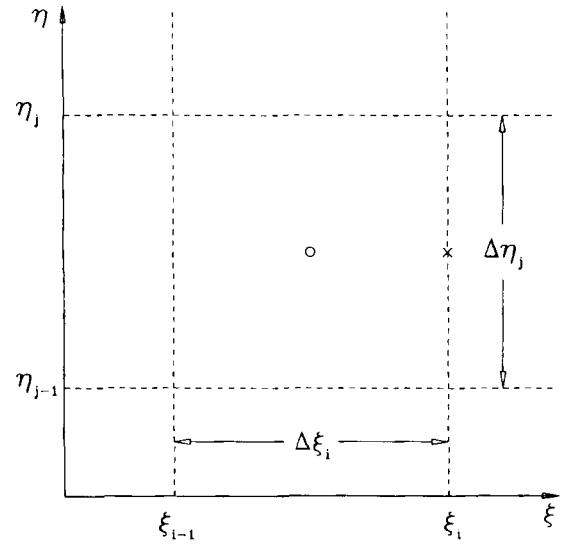

Figure 1. The computational grid used for the Keller box method. The variables η and ξ are the transformed cross-stream and streamwise co-ordinates respectively

for the momentum equation. These equations are then differenced within a single grid mesh, with no differencing across grid boundaries. This allows non-uniform grid spacings to be used in a very natural way. Central differences are employed throughout the scheme. The computational grid that is used for both the Keller box and the upstream Keller box methods is shown in Figure 1. Equations with streamwise derivatives are centred on a point at the geometric centre of the mesh (circle in Figure 1) and equations that do not have streamwise derivatives are centred at the midpoint of the unknown's boundary (cross in Figure 1). This system of equations is then linearized using Newton's method and solved iteratively. The method has been thoroughly studied with regard to its stability and the error is known to be second-order in $\Delta\xi$ and $\Delta\eta$.[7]

The Keller box differencing scheme was attempted, but because of streamwise averaging an annoying oscillation was retained in the axial pressure gradient for developing pipe flow. This oscillation was less that 1% of the mean pressure gradient, but it caused an alternating sign radial velocity distribution that was retained in the fully developed flow region.

When $f(x) = 1$, equations (1), (2) and (4) yield the following non-linear system of equations if the standard Keller box differencing scheme is used:

$$\left(\frac{1}{2\Delta\xi}\right)(U_j + U_{j-1} - U_j^{\mathrm{p}} - U_{j-1}^{\mathrm{p}}) = \left(\frac{1}{(\eta_j + \eta_{j-1})\Delta\eta}\right)[\eta_{j-1}(V_{j-1} + V_{j-1}^{\mathrm{p}}) - \eta_j(V_j + V_j^{\mathrm{p}})], \quad (5)$$

$$\left(\frac{U_j + U_{j-1} + U_j^{\mathrm{p}} + U_{j-1}^{\mathrm{p}}}{4}\right)\left(\frac{U_j + U_{j-1} - U_j^{\mathrm{p}} - U_{j-1}^{\mathrm{p}}}{2\Delta\xi}\right) + \left(\frac{V_j + V_{j-1} + V_j^{\mathrm{p}} + V_{j-1}^{\mathrm{p}}}{4}\right)\left(\frac{W_j + W_{j-1} + W_j^{\mathrm{p}} + W_{j-1}^{\mathrm{p}}}{4}\right) = -\frac{1}{\rho}\frac{dP}{d\xi} + \frac{\nu[\eta_j(W_j + W_j^{\mathrm{p}}) - \eta_{j-1}(W_{j-1} + W_{j-1}^{\mathrm{p}})]}{(\eta_j + \eta_{j-1})\Delta\eta}, \quad (6)$$

$$\frac{W_j + W_{j-1}}{2} = \frac{U_j - U_{j-1}}{\Delta\eta}. \quad (7)$$

The values at the previous step are indicated by the superscript 'p', and the subscripts j and $j-1$ indicate the cross-stream location as shown in Figure 1. The second term of the left-hand side of equation (2) could also be approximated by

$$\frac{V_j W_j + V_{j-1} W_{j-1} + V_j^{\mathrm{p}} W_j^{\mathrm{p}} + V_{j-1}^{\mathrm{p}} W_{j-1}^{\mathrm{p}}}{4}.$$

Keller has noted that either approximation will produce similar results. Notice that the terms involving cross-stream derivatives of the original differential equations are averaged over the known and unknown faces of the difference box, hence the system of equations will yield results that are correct in the average. At first glance this would appear to smooth the resultant solution. However, this is not true: if the known or initial values were in error, the resultant solution at the next step would have an error of opposite sign sufficient to compensate for the initial error. When this system of equations has been used to compute entrance flow in a pipe it has been observed to produce oscillations in the computed radial velocity distributions where the flow should be fully developed—a radial velocity distribution at one station followed by a radial velocity distribution of opposite sign at the next station. This continued for as long as the computations were carried out; the radial velocity distribution would not decay to zero as it should.

The previous discussion about the Keller box method has been restricted to one box. The flow quantities at each node are tied together by having a connection with two adjacent boxes. This

complicates the analysis of the system of equations that is generated in this algorithm. However, the averaging of flow quantities at two streamwise locations still smooths out errors and oscillations before balancing the thin shear layer equations. The average value of the solution may be correct, but the solutions at the upstream and downstream faces of the step could be incorrect.

Equations (5) and (6) can be reduced to a single equation if the radial velocity distributions have been assumed to oscillate in sign but not in magnitude from step to step. If we assume this behaviour for the radial velocity distributions, the following approximation to equation (2) results:

$$\frac{1}{\rho}\frac{dP}{d\xi} = \frac{\nu[\eta_j(W_j + W_j^p) - \eta_{j-1}(W_{j-1} + W_{j-1}^p)]}{(\eta_j + \eta_{j-1})\Delta\eta}. \tag{8}$$

The system of differential equations is now approximated by this equation and equation (7). Both of these equations appear to be valid approximations to the differential equations for fully developed pipe flow. However, the assumption about the radial velocity distributions is not valid for this flow. For a fixed value of the pressure gradient, equation (8) will have a correct average solution. Equation (7) will compute a U-distribution based on upstream values of W. This will result in a different axial velocity distribution at the upstream face if the initial W-distribution is only approximately fully developed. The pressure gradient will have to be changed and the calculations repeated iteratively to conserve mass flux for an internal flow. If the distributions are slightly different from those for a fully developed flow, the pressure gradient will have to be adjusted to compensate for the resultant error at the upstream face. The cross-stream regions where the initial distribution is high will be made into regions where the computed distribution is low, and similarly for the initially low regions. This will be repeated in kind at the next step, and the pressure gradient and the velocity distribution will oscillate about an average value. The correct solution can be recovered by averaging the pressure gradient and distributions at adjacent steps.

It is much more difficult to evaluate what happens for evolving flows. However, we can observe that the interaction of adjusting the pressure gradient and computing the averaged flow will cause oscillations to ride on the correct streamwise pressure gradient. In flows where there is a large change in pressure gradient from step to step the oscillations will also be large and as a result the sign of the pressure gradient may change periodically. This will yield axial velocities that change sign near the walls of the duct if the amplitude of the oscillation is large enough. Averaging the solutions between adjacent steps is not a suitable solution for a flow that is evolving, since the streamwise evolution will be smeared out.

The previous argument illustrates that the oscillation for fully developed pipe flow is algebraic in nature. This would lead us to conclude that the averaging of $\partial U/\partial x$ at two cross-stream locations would cause an oscillation in that direction. This would be generally true if the value of this derivative was not precisely known at the wall, where U is specified. The value of $\partial U/\partial x$ at the location next to the wall is more restricted, and its error is only due to approximation and round-off. If this location is sufficiently close to the wall, the approximation error can be made very small. Hence we should not expect an algebraic oscillation unless the grid is too coarse.

Gresho and Lee[8] suggest that it is inappropriate to develop *a priori* numerical methods to suppress oscillations. They argue that the oscillations in the conventional finite element methods are a strong indication about the accuracy of the simulation and should only be eliminated by grid refinement in critical regions and careful application of the boundary conditions. Artificial damping is seen to mask the underlying physics of the flow being examined. In the methods that they discussed, wiggles in the computed flow distributions could be eliminated generally by

applying a finer approximation. This is not possible for the Keller box method since the oscillation is due to the algebraic averaging and will remain regardless of grid resolution. The computed values are smoothed before the thin shear layer equations are balanced. In terms of control theory the feedback signal is so strongly damped that the output response can oscillate.

The differencing scheme that successfully approximated fully developed pipe flow used upwind differencing to approximate the streamwise derivatives (see Patankar[9] for a discussion on central and upwind differencing in a general context), with all the equations approximated on a point centred at the edge of the box where the unknown values were—the cross in Figure 1. The accuracy of the solution will then be first-order in the streamwise direction $\Delta\xi$. The raw system of difference equations is non-linear and cannot be solved directly. This non-linear system can be linearized by substituting a guessed value and a correction value for the unknown, then solving for the correction after ignoring the quadratic terms. Keller[10] has pointed out that solving for the corrections has the advantage of reducing cancellation errors. This results in a block tridiagonal system of equations which can be easily solved. The initial guess for the unknowns was set equal to their value at the upstream location, and the system was repeatedly iterated until the corrections were sufficiently small. The value of W at the wall was found to vary the most from iteration to iteration. Hence when its correction was less than 10^{-6} of the mean radial derivative of the axial velocity the iterations were stopped.

It is interesting to examine the new difference scheme for fully developed pipe flow to see if it is consistent with the true physics of the flow. When $f(x) = 1$, equations (1), (2) and (4) yield the following non-linear system of equations when this differencing scheme is used:

$$\left(\frac{1}{2\Delta\xi}\right)(U_j + U_{j-1} - U_j^p - U_{j-1}^p) = \left(\frac{2}{(\eta_j + \eta_{j-1})\Delta\eta}\right)(\eta_{j-1}V_{j-1} - \eta_j V_j), \tag{9}$$

$$\left(\frac{U_j + U_{j-1}}{2}\right)\left(\frac{U_j + U_{j-1} - U_j^p - U_{j-1}^p}{2\Delta\xi}\right) + \left(\frac{V_j + V_{j-1}}{2}\right)\left(\frac{W_j + W_{j-1}}{2}\right) = -\frac{1}{\rho}\frac{dP}{d\xi} + \frac{2\nu(\eta_j W_j - \eta_{j-1}W_{j-1})}{(\eta_j + \eta_{j-1})\Delta\eta}, \tag{10}$$

$$\frac{W_j + W_{j-1}}{2} = \frac{U_j - U_{j-1}}{\Delta\eta}. \tag{11}$$

An alternating sign V-distribution cannot satisfy (9) if the flow is fully developed, hence the radial velocities have to go to zero. Equation (10) then becomes

$$\frac{1}{\rho}\frac{dP}{d\xi} = \frac{2\nu(\eta_j W_j - \eta_{j-1}W_{j-1})}{(\eta_j + \eta_{j-1})\Delta\eta}. \tag{12}$$

Here the values of W are fixed by the pressure gradient term. This scheme is a much better approximation to the thin shear layer equations for fully developed flow.

The pressure gradient for an internal flow is not known *a priori*; it is one of the unknowns and it must be set to a value that satisfies conservation of mass in the duct. The derivative of the difference equations for the corrections to the flow variables U, V and W gives a linear block tridiagonal system of equations. The solution to this system can be used to solve for the pressure gradient.[11,12] First the estimated axial velocity distribution was numerically integrated to find the computed flow rate. Then the derivative of the axial velocity with respect to the pressure gradient was integrated to find the rate of change of mass flux with respect to the pressure gradient. An improved value of the pressure gradient was then computed using a Newton scheme

with the old pressure gradient, the actual mass flux, the estimated mass flux and the rate of change of mass flux, i.e.

$$\left(\frac{dP}{d\xi}\right)^{\text{new}} = \left(\frac{dP}{d\xi}\right)^{\text{old}} - \frac{m_{\text{actual}} - m_{\text{estimated}}}{\dot{m}}. \tag{13}$$

The initial guess for the pressure gradient was set equal to the pressure gradient at the previous step and the equations were iterated until the estimated mass flux was within 10^{-6} of the actual mass flux. It should be noted that to obtain this kind of accuracy the numerical quadrature formula has to be very carefully chosen. For this work, cubic spline integration was selected.

The overall iteration scheme was as follows. An initial guess of the pressure gradient, the velocities and W was made using the values from the previous axial step. For the first step the initial guessed pressure gradient was zero. Using the guessed value of the pressure gradient the velocity calculations were iterated to the accuracy stated, then the pressure gradient was updated. If the computed mass flux was satisfactory the iterations stopped, otherwise the new values of the pressure gradient, the velocities and W were treated as an initial guess and the iteration scheme was repeated. The total number of iterations is a function of how rapidly the flow is changing in the streamwise direction. For the first step in developing pipe flow, roughly 25 iterations of velocity and pressure gradient were required, and for the fully developed region, three iterations would suffice. These iteration counts could be improved by choosing a better initial guess; most of the iterations were done getting the pressure gradient.

A problem with the calculations arises at the first axial step that is not apparent from the previous discussion. The calculations become unstable if the first step is not sufficiently large. This is the result of the elliptic character of the flow near the wall at the inlet of a pipe and the interaction with the pressure gradient. In this region the $\partial^2 U/\partial x^2$ term in the thin shear layer equations is not negligible. This can be minimized by using transformed co-ordinates near the inlet or by making the first step larger. It is easier to use a larger first step than to switch between transformed co-ordinates, so that was the strategy that was employed. The larger step makes the thin shear layer approximation a better approximation over the step.

3. EXAMPLE FLOWS

Two example flows were selected to test this computational method: entrance flow in a pipe and flow in a 2° conical diffuser. The entrance flow in a pipe has been thoroughly examined experimentally and theoretically, thus providing a good benchmark for the method. The 2° conical diffuser has not been extensively studied. However, this flow gives a good indication of the method's behaviour in adverse pressure gradients.

Developing pipe flow

Laminar flow in the entrance of a circular pipe has been extensively studied by a variety of methods. Qualitatively, the axisymmetric and two-dimensional entrance flow problems are very similar in nature. Hence results for the two-dimensional flow will also be considered in this discussion. The inlet condition used for most experimental studies is that from a gently contracting bell mouth which produces a nearly uniform axial velocity distribution at the entrance to the pipe. From this point a boundary layer grows on the inside surface and at some point the boundary layers from opposite sides of the pipe merge. The mass flux at any cross-section must be constant if no fluid is injected or extracted through the walls. This condition is obtained by the pressure gradient being a function of the axial position. Near the inlet the rate of

change of the displacement thickness is largest and thus the pressure gradient is also largest there. At the wall at the very beginning of the pipe the magnitude of $\partial^2 U/\partial x^2$ is not negligible and the flow near this point is elliptic. However, this region is very small so an analysis using the boundary layer equations should not be severely in error. Eventually the velocity distribution becomes the well known Poiseuille flow. From this point on the velocities and the pressure gradient are constant.

Analytic solutions have been obtained using a variety of assumptions about the initial conditions. The initial flow could have a uniform velocity across the inlet or the initial flow could be that from a stream tube. The earliest studies employed boundary layer theory by assuming that the core flow is uniform at each cross-section and that the core is accelerated by the boundary layer displacement. This type of analysis is thoroughly described in References 13 and 14. The solutions obtained from this type of analysis are not valid very near the inlet or where the boundary layers start to merge. These studies provided qualitatively correct flow characteristics but inadequate detailed features. More precise results for the entry flow problem have been obtained by Van Dyke[15] and Wilson[16, 17] using asympototic expansions. The result of these inquiries agree with numerical solutions of the full Navier–Stokes equations. Van Dyke pointed out that the usual assumption of a uniform velocity at the inlet for a channel is not correct. The flow near the inlet doest not have an accelerated uniform core owing to displacement. This is the result of the flow at the inlet being influenced by the downstream flow inside the pipe. Numerical solutions[18–20] using the full Navier–Stokes equations have shown that the axial velocity has a maximum away from the centreline at cross-sections near the inlet. This shows that comparisons between experimental data and computations have to be made with some care since the initial conditions could be different. This will not be a factor in the developed region but will influence the development lengths.

The laminar flow entrance flow of air in a pipe was computed using this computational scheme. The inside diameter of the pipe was 10 cm. A uniform velocity distribution was assumed to exist at the inlet, i.e. $U = 0{\cdot}155\ \mathrm{m\,s^{-1}}$ and $V = 0{\cdot}0\ \mathrm{m\,s^{-1}}$. Fifty grid points were geometrically distributed along a radius, where the distance between adjacent pairs of grids differed by a factor of 1·02. The distance between the grids was smallest next to the wall and increased in length on

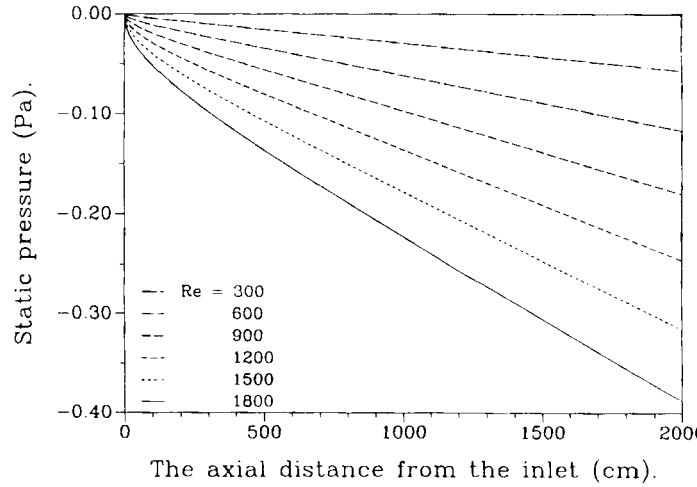

Figure 2. The static pressure distribution in the pipe. The inlet flow was a uniform velocity distribution and the inlet diameter was 10 cm. The fluid was air at room temperature

moving towards the centreline. The total length of the computational domain was 20 m, with 1 cm steps for the first 10 cm and 10 cm steps for the remainder.

The flow was computed for Reynolds numbers ranging from 100 to 1800 in steps of 100. The static pressure, pressure gradient, skin friction and centreline velocity for these calculations are given in Figures 2–5 respectively for Reynolds numbers of 300, 600, 900, 1200, 1500 and 1800. Detailed velocity distributions for a Reynolds number of 1000, which corresponds to a mean velocity of 0·155 m s^{-1}, are given in Figure 6 for the axial velocities and in Figure 7 for the radial velocities.

The static pressure was nearly linear except in the first 45 diameters of the pipe for a Reynolds number of 1800. The pressure gradient and the skin friction increased rapidly to their final fully developed values. The pressure gradient was near the fully developed value at roughly 70

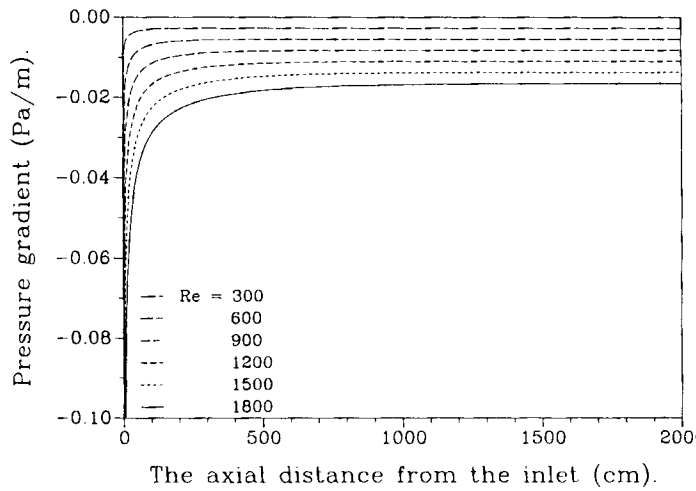

Figure 3. The pressure gradient distribution in the pipe. The conditions are the same as in Figure 2

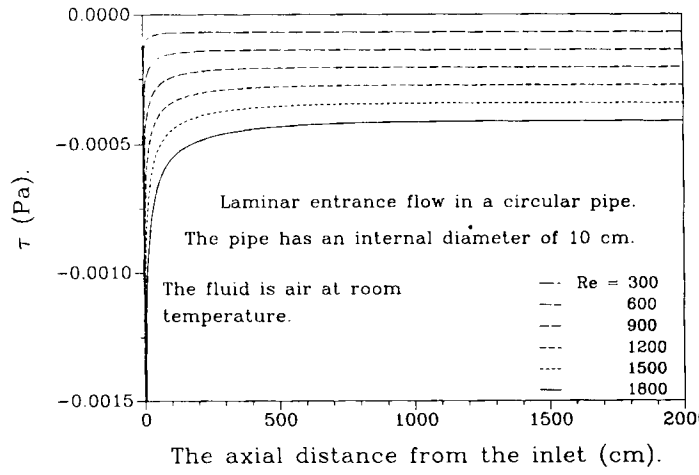

Figure 4. The skin friction distribution in the pipe. The conditions are the same as in Figure 2

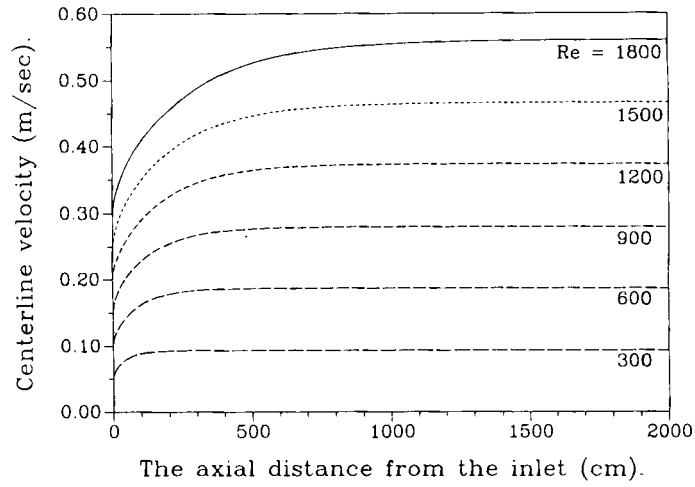

Figure 5. The centreline velocity within the pipe. The conditions are the same as in Figure 2

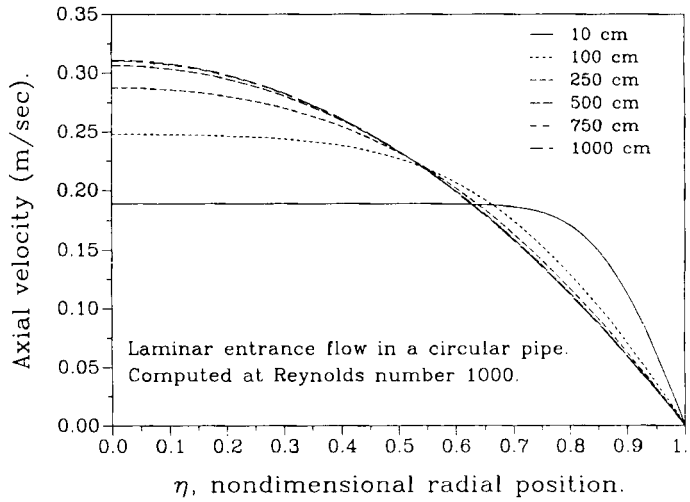

Figure 6. The axial velocity distributions in the inlet region of the pipe. The conditions are the same as in Figure 2; $Re = 1000$

diameters and the skin friction at roughly 50 diameters. The centreline velocity increased at much slower rate; it came within 99% of the fully developed value at roughly 85 diameters. This suggests that when the entrance length is being considered one has to be very careful of what measure is going to be used, since widely varying lengths will result. The entrance length increases rapidly with Reynolds number regardless of what is being used to indicate that the flow is fully developed. No calculations have been made to see if the ratio of entrance lengths based on two different indicators is a function of the Reynolds number.

The axial velocity distributions evolved very rapidly in the initial regions of the flow, where the largest changes to the velocity occurred in the central portion of the duct. As expected, the central core of the entrance flow is uniform in the entrance of the pipe. However, this is only true within roughly 25 diameters of the inlet. Farther downstream, in the central core of the flow, the axial

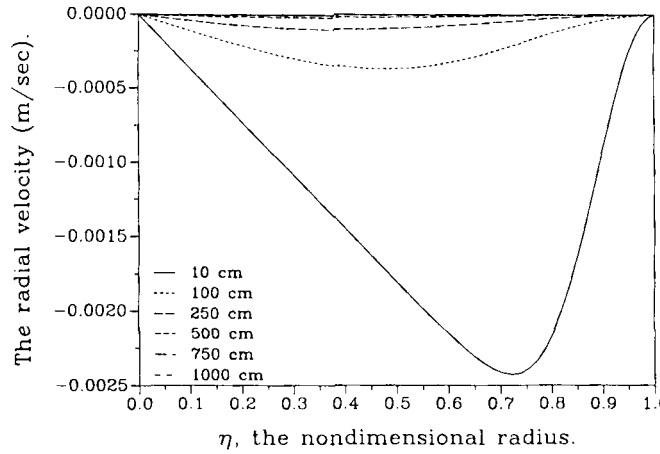

Figure 7. The radial velocity distributions in the inlet region of the pipe. The conditions are the same as in Figure 2; $Re = 1000$. Notice that the distributions for 750 and 1000 cm are essentially zero

velocities accelerate rapidly in the streamwise direction when compared with the fluid near the wall, which decelerates slowly.

The radial velocities were very small throughout the pipe, less than 2·5 mm s^{-1}. Hence the flow is very nearly parallel to the axis. Additionally, the magnitude of the radial velocities goes to zero very rapidly in the streamwise direction. Throughout the pipe they varied linearly with the radius in the central core of the duct. They appear to vary quadratically with the distance from the wall, very near the wall. An interesting feature of this computational method can be seen from the radial velocity distribution. The system of equations only allows three boundary conditions to be set—the centreline values of the radial velocity and W, and the wall axial velocity. Hence there is no way to force the wall radial velocity to any prescribed value without allowing one of the other variables to vary. All the calculations show that the wall radial velocities asymptotically go to zero, the correct value for impermeable walls.

Since the numerical model used in this set of computations is based on the thin shear layer equations, the results cannot reflect the elliptic character of the flow near the wall at the inlet or the upstream influence of the flow inside the pipe. Considering this, the scheme still produces results that are of sufficient precision for most practical purposes.

The 2° conical diffuser

A 2° conical diffuser is formed by the frustrum of a cone with a 2° included angle. The flow is characterized by increasing pressure and decreasing velocity in the downstream direction. It is generally known that the flow is strongly dependent on the inlet conditions, in effect the displacement thickness along the pipe walls that feed the diffuser inlet.

An analytic solution for the self-similar region of the flow far downstream of the inlet between two diverging planes is known, the Jeffery–Hamel flow.[21] In this region of the flow the velocity distributions are self-similar. The Navier–Stokes equations then degenerate to a second-order, non-linear ordinary differential equation over the surface. The solution to this equation shows that, for a fixed angle between the plates, the flow is purely outflow for Reynolds numbers below a critical value and is a mixture of inflow and outflow above that value. This critical value is a function of the angle between the plates.

There is no generally known self-similar solution for the conical diffuser, and since the influence of the geometric differences between these flows is not known, one cannot expect the Jeffery–Hamel flow results to be applicable. The qualitative character should be similar, i.e. one could expect that for a sufficiently low Reynolds number one would have an attached flow and that for Reynolds numbers above a critical value one would find separation regions. One of the difficulties of examining these types of flow can be explained by considering the Jeffery–Hamel flow. Near the critical Reynolds number there is the real possibility that the flow will detach from one wall but remain attached to the other, i.e. the flow becomes non-symmetric. Additional problems arise in that oscillations in time may also occur near and above the critical Reynolds number. These difficulties are discussed by Johnston[22] with specific regard to turbulent flows.

All the computations were for a diffuser with an inlet 10 cm in diameter and a total length of 200 cm, with air at standard temperature and pressure as the fluid. The initial flow was that from a 2 m pipe, as computed in the previous section. This caused the initial velocity distribution being fed into the diffuser to be fully developed pipe flow. The static pressure, pressure gradient, skin friction and centreline velocity are given in Figures 8–11 respectively for Reynolds numbers ranging from 100 to 1800 in steps of 100, except where noted. Additionally, velocity distributions at various steamwise locations are given for a Reynolds number of 1000 in Figure 12 for the axial velocities and in Figure 13 for the radial velocities.

The static pressure and pressure gradient distributions are more interesting for the 2° conical diffuser than for the entrance region in the pipe. Looking at the static pressure, Figure 8, one can see that the character of the distributions changes with the Reynolds number. At the lower Reynolds numbers the static pressure remains negative with respect to the pressure at the inlet.

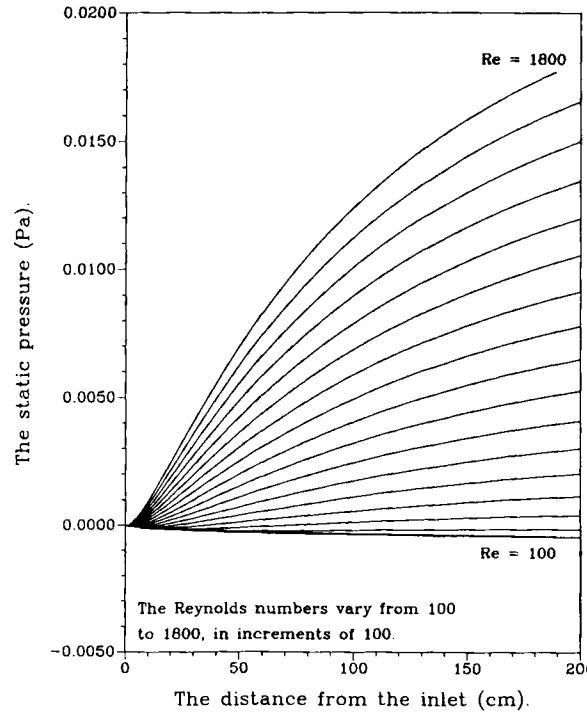

Figure 8. The static pressure distribution in the 2° conical diffuser. The inlet flow was from fully developed pipe flow and the inlet diameter was 10 cm

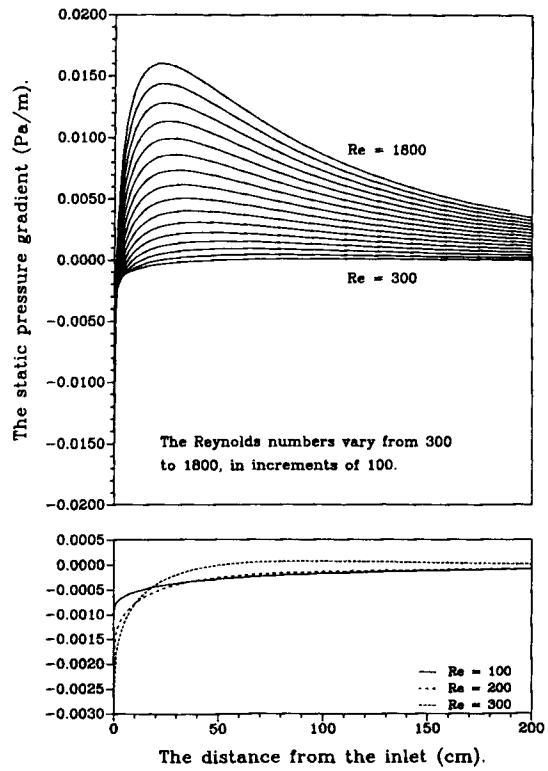

Figure 9. The pressure gradient in the 2° conical diffuser. The conditions are the same as in Figure 8

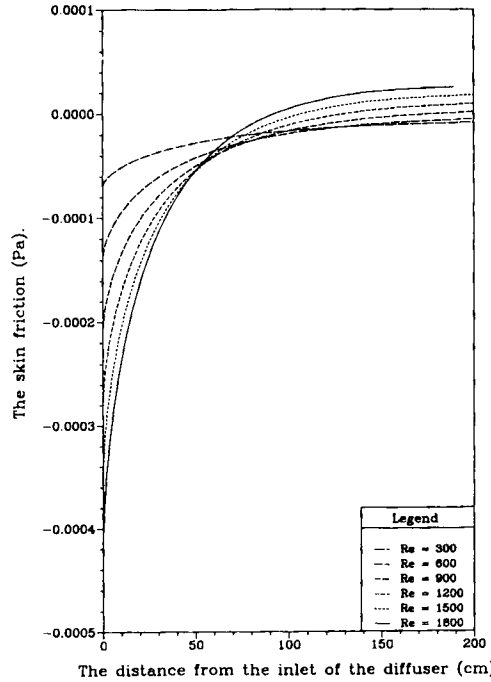

Figure 10. The wall skin friction in the 2° conical diffuser. The conditions are the same as in Figure 8

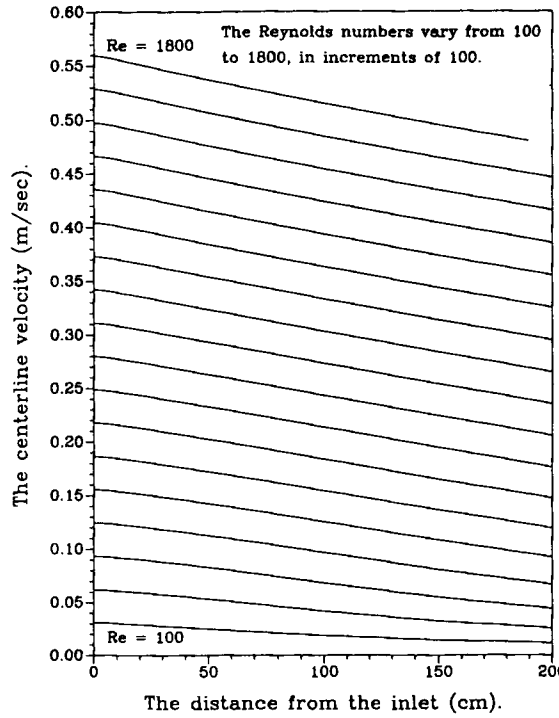

Figure 11. The centreline velocity distribution in the 2° conical diffuser. The conditions are the same as in Figure 8

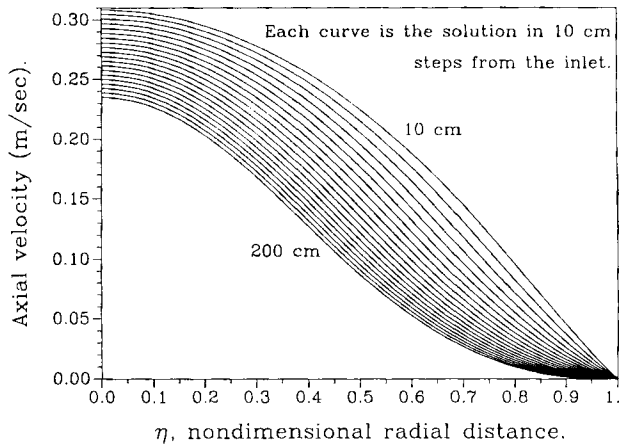

Figure 12. The axial velocity distributions in the 2° conical diffuser. The conditions are the same as in Figure 8; $Re = 1000$

This is evident for Reynolds numbers of 100, 200 and 300, where the pressure gradient, Figure 9, is negative throughout the diffuser. For Reynolds numbers above 300 the pressure gradient is positive throughout the diffuser. At these higher Reynolds numbers the pressure gradient also has a maximum value located at roughly five inlet diameters into the diffuser, and this characteristic becomes more exaggerated as the Reynolds number increases. Hence the pressure recovery and efficiency of this diffuser will depend heavily upon the Reynolds number.

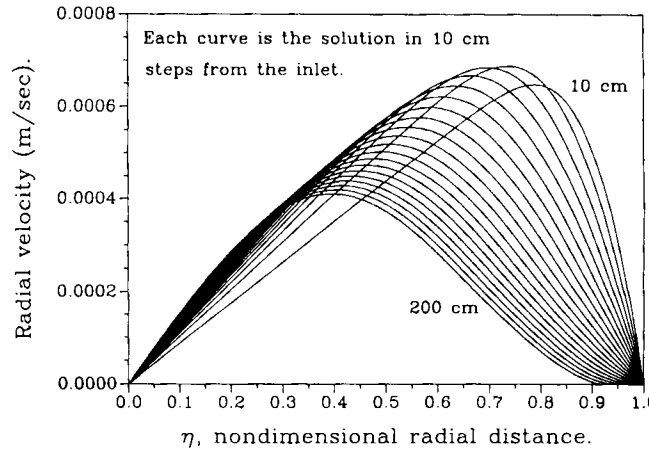

Figure 13. The radial velocity distributions in the 2° conical diffuser. The conditions are the same as in Figure 8; $Re = 1000$

The wall skin friction, Figure 10, indicates that the flow separates at the end of the diffuser at a Reynolds number of 900. For larger Reynolds numbers the positive skin friction zone creeps upstream into the diffuser and the size of this region increases with Reynolds number. Since no special care was taken to account for separation, one has to be exceedingly careful about drawing any conclusions about the flow in this region. It does appear that the numerical scheme does tolerate a limited amount of reverse flow without becoming unstable. The calculations were stopped when the Reynolds number was 1800 since they became unstable near the outlet of the diffuser. This might be corrected by using the FLAIR approximation.

The centreline velocity distribution, Figure 11, for all Reynolds numbers was nearly linear throughout the diffuser.

The axial velocity distributions at a Reynolds number of 1000 are given at 10 cm steps through the diffuser in Figure 12. In the central core of the flow the distributions are very similar for the entire diffuser. However, the wall region went from being weakly concave down near the inlet to concave up near the outlet. There is a small region for the last few steps where the flow is reversed, but the scale of the graph hides this feature. The radial velocity distributions are given at the same locations in the diffuser for a Reynolds number of 1000 in Figure 13. In the central core of the flow the radial velocity distribution is nearly linear with radius. Near the wall the flow again appears to vary quadratically with the distance from the wall. At this Reynolds number the magnitude of the radial velocities is very small, less than 1 mm s^{-1}. Thus the flow is nearly parallel in the diffuser as well, which validates the use of the thin shear layer equations *a posteriori*. The maximum value of the radial velocity at a given location moves from the wall towards the centreline, proportionate to the local radius. Finally, the radial velocities asymptotically approach zero as the wall is approached. This boundary condition was not set by the differential equations but is a consequence of conservation of mass.

4. CONCLUSIONS

The numerical scheme described in this paper yields reasonably accurate results for flows inside axisymmetric ducts. It corrects a problem with oscillation that arises using the Keller box method and it is simpler to use than a full Navier–Stokes finite difference scheme.

ACKNOWLEDGEMENT

The author would like to acknowledge the financial support of the Natural Sciences and Engineering Research Council of Canada.

APPENDIX: THE MODIFIED EQUATIONS

The grid used for the finite difference scheme is shown in Figure 1. The following equations use the standard notation for the velocities, pressure gradient, density and viscosity. When reference is made to a known upstream variable it is indicated with a superscript 'p'.

The modified equations still generate a block tridiagonal system of equations, of a form given by

$$\begin{bmatrix} \mathbf{A}_1 & \mathbf{C}_1 & \mathbf{0} & \mathbf{0} & \mathbf{0} \\ \mathbf{B}_2 & \mathbf{A}_2 & \mathbf{C}_2 & \mathbf{0} & \mathbf{0} \\ \mathbf{0} & \mathbf{B}_3 & \mathbf{A}_3 & \mathbf{C}_3 & \mathbf{0} \\ \mathbf{0} & \mathbf{0} & \mathbf{B}_4 & \mathbf{A}_4 & \mathbf{C}_4 \\ \mathbf{0} & \mathbf{0} & \mathbf{0} & \mathbf{B}_5 & \mathbf{A}_5 \end{bmatrix} \begin{bmatrix} \delta\mathbf{X}_1 \\ \delta\mathbf{X}_2 \\ \delta\mathbf{X}_3 \\ \delta\mathbf{X}_4 \\ \delta\mathbf{X}_5 \end{bmatrix} = \begin{bmatrix} \mathbf{R}_1 \\ \mathbf{R}_2 \\ \mathbf{R}_3 \\ \mathbf{R}_4 \\ \mathbf{R}_5 \end{bmatrix}$$

for a five-node grid. The submatrices are 3×3 matrices for a laminar flow.

For the kth interval the submatrices can be written as

$$\mathbf{B}_k = \begin{bmatrix} b_{11}^k & b_{12}^k & b_{13}^k \\ b_{21}^k & b_{22}^k & b_{23}^k \\ b_{31}^k & b_{32}^k & b_{33}^k \end{bmatrix}, \qquad \mathbf{A}_k = \begin{bmatrix} a_{11}^k & a_{12}^k & a_{13}^k \\ a_{21}^k & a_{22}^k & a_{23}^k \\ a_{31}^k & a_{32}^k & a_{33}^k \end{bmatrix},$$

$$\mathbf{C}_k = \begin{bmatrix} c_{11}^k & c_{12}^k & c_{13}^k \\ c_{21}^k & c_{22}^k & c_{23}^k \\ c_{31}^k & c_{32}^k & c_{33}^k \end{bmatrix}, \qquad \mathbf{R}_k = \begin{bmatrix} r_1^k \\ r_2^k \\ r_3^k \end{bmatrix}, \qquad \mathbf{X}_k = \begin{bmatrix} \delta U^k \\ \delta V^k \\ \delta W^k \end{bmatrix}.$$

Thin shear layer equations

The values of the elements of the various matrices are given by the following formulae:

$$a_{11}^k = \frac{\eta_k U_k}{2f^2(\xi)\Delta\xi} + \frac{f'(\xi)\eta_k^2 W_k}{2f^3(\xi)}, \qquad a_{12}^k = \frac{\eta_k W_k}{2f(\xi)}, \qquad a_{13}^k = \frac{\eta_k V_k}{2f(\xi)} - \frac{\eta_k v_k}{\Delta\eta_k} + \frac{f'(\xi)\eta_k^2 U_k}{2f^3(\xi)},$$

$$a_{21}^k = \frac{-1}{\Delta\eta_k}, \qquad a_{22}^k = 0, \qquad a_{23}^k = \frac{-1}{2},$$

$$a_{31}^k = \frac{\eta_{k+1} + \eta_k}{4f(\xi)\Delta\xi}, \qquad a_{32}^k = \frac{-\eta_k}{\Delta\eta_{k+1}}, \qquad a_{33}^k = \frac{(\eta_{k+1} + \eta_k)^2 f'(\xi)}{8f^3(\xi)},$$

$$b_{11}^k = \frac{\eta_{k-1} U_{k-1}}{2f^2(\xi)\Delta\xi} + \frac{f'(\xi)\eta_{k-1}^2 W_{k-1}}{2f^3(\xi)}, \qquad b_{12}^k = \frac{\eta_{k-1} W_{k-1}}{2f(\xi)},$$

$$b_{13}^k = \frac{\eta_{k-1} V_{k-1}}{2f(\xi)} + \frac{\eta_{k-1} v_{k-1}}{\Delta\eta_k} + \frac{f(\xi)\eta_{k-1}^2 U_{k-1}}{2f^3(\xi)},$$

$$b_{21}^k = \frac{-1}{\Delta\eta_k}, \qquad b_{22}^k = 0, \qquad b_{23}^k = \frac{-1}{2},$$

$$b_{31}^k = b_{32}^k = b_{33}^k = c_{11}^k = c_{12}^k = c_{13}^k = c_{21}^k = c_{22}^k = c_{23}^k = 0,$$

$$c_{31}^k = \frac{\eta_k + \eta_{k-1}}{4f(\xi)\Delta\xi}, \qquad c_{32}^k = \frac{-\eta_{k-1}}{\Delta\eta_k}, \qquad c_{33}^k = \frac{(\eta_k + \eta_{k-1})^2 f'(\xi)}{8f^2(\xi)},$$

$$r_1^k = \frac{\eta_k v_k W_k - \eta_{k-1} v_{k-1} W_{k-1}}{\Delta\eta_k} - \frac{(\eta_k + \eta_{k-1})}{2\rho f^2(\xi)} \frac{dP}{d\xi} - \frac{\eta_k V_k W_k + \eta_{k-1} V_{k-1} W_{k-1}}{2f(\xi)}$$
$$- \frac{f'(\xi)}{2f^3(\xi)}(\eta_k^2 U_k W_k + \eta_{k-1}^2 U_{k-1} W_{k-1}) - \frac{1}{4f^2(\xi)\Delta\xi}[\eta_k(U_k^2 - U_k^{P2}) + \eta_{k-1}(U_{k-1}^2 - U_{k-1}^{P2})],$$

$$r_2^k = \frac{1}{2}(W_k + W_{k-1}) - \frac{1}{\Delta\eta_k}(U_k - U_{k-1}),$$

$$r_3^k = \frac{\eta_k V_k - \eta_{k+1} V_{k+1}}{\Delta\eta_{k+1}} - \frac{\eta_{k+1} + \eta_k}{4f(\xi)\Delta\xi}(U_{k+1}^P + U_k^P - U_{k+1} - U_k) - \frac{(\eta_{k+1} + \eta_k)^2 f'(\xi)}{8f^2(\xi)}(W_{k+1} + W_k).$$

Boundary conditions

The symmetry condition $W = 0$ on the axis of symmetry:

$$a_{11}^1 = a_{12}^1 = c_{11}^1 = c_{12}^1 = c_{13}^1 = r_1^1 = 0, \qquad a_{13}^1 = 1.$$

The radial velocity $V = 0$ on the axis of symmetry:

$$a_{21}^1 = a_{23}^1 = c_{21}^1 = c_{22}^1 = c_{23}^1 = r_2^1 = 0, \qquad a_{22}^1 = 1.$$

The no slip condition $U = 0$ at the wall:

$$a_{31}^N = 1, \qquad a_{32}^N = a_{33}^N = b_{31}^N = b_{32}^N = b_{33}^N = 0.$$

Sensitivity to the pressure gradient

The equations that are used to compute the derivatives of U, V and W with respect to the pressure gradient are identical, with the following single exception:

$$r_1^k = -\frac{(\eta_k + \eta_{k-1})}{2\rho f^2(\xi)} \frac{dP}{d\xi}.$$

The derivative of U is then integrated over the cross-section to give $\dot{m}$.

REFERENCES

1. P. G. Williams, 'A reverse flow computation in the theory of self-induced separation', in R. D. Richtmyer (ed.), *Proc. Fourth Int. Conf. on Numerical Methods in Fluid Dynamics; Lecture Notes in Physics, Vol. 35*, Springer, Berlin, 1975, pp. 445–451.
2. H. B. Keller, 'Some computational problems in boundary layer flows', in R. D. Richtmyer (ed.), *Proc. Fourth Int. Conf. on Numerical Methods in Fluid Dynamics; Lecture Notes in Physics, Vol.* 35, Springer, Berlin, 1975, pp. 1–21.
3. T. Cebeci and A. M. O. Smith, *Analysis of Turbulent Boundary Layers*, Academic Press, New York, 1974, pp. 265–280.
4. T. Cebeci and P. Bradshaw, *Momentum Transfer in Boundary Layers*, McGraw-Hill, New York, 1977, pp. 213–218.
5. P. Bradshaw, T. Cebeci and J. H. Whitelaw, *Engineering Calculation Methods for Turbulent Flow*, Academic Press, London, 1981, pp. 88–92.
6. D. A. Anderson, J. C. Tannehill and R. H. Pletcher, *Computational Fluid Mechanics and Heat Transfer*, McGraw-Hill, New York, 1984, pp. 349–354.
7. H. B. Keller, 'Accurate difference methods for nonlinear two-point boundary value problems', *SIAM J. Numer. Anal.*, **11**, 305–320 (1974).
8. P. M. Gresho and R. L. Lee, 'Don't suppress the wiggles—they're telling you something', *Comput. Fluids*, **9**, 223–253 (1981).
9. S. V. Patankar, *Numerical Heat Transfer and Fluid Flow*, McGraw-Hill, New York, 1980, pp. 80–85.

10. H. B. Keller, 'Numerical methods in boundary-layer theory', in J. L. Lumley, M. Van Dyke, M. and H. L. Read, (eds), *Annual Reviews in Fluid Mechanics*, Annual Reviews Inc., Palo Alto, CA, 1978, p. 422.
11. G. D. Raithby and G. E. Schneider, 'Numerical solution of problems in incompressible fluid flow: treatment of the velocity–pressure coupling', *Numer. Heat Transfer*, **102,** 417–440 (1979).
12. D. A. Anderson, J. C. Tannehill and R. H. Pletcher, *Computational Fluid Mechanics and Heat Transfer*, McGraw-Hill, New York, 1984, pp. 382–389.
13. S. Goldstein, *Modern Developments in Fluid Dynamics, Vol. I*, Dover, New York, 1965, pp. 299–309.
14. L. Rosenhead, *Laminar Boundary Layers*, Dover, New York, 1988, pp. 439–446.
15. M. Van Dyke, 'Entry flow in a channel', *J. Fluid Mech.*, **44,** 813–823 (1970).
16. S. Wilson, 'The development of Poiseuille flow', *J. Fluid Mech.*, **38,** 793–806 (1969).
17. S. Wilson, 'Entry flow in a channel. Part 2', *J. Fluid Mech.*, **46,** 787–799 (1971).
18. Y. L. Wang and P. A. Longwell, 'Laminar flow in the inlet section of parallel plates', *AIChE J.*, **10,** 323–329 (1964).
19. B. Atkinson, M. P. Brocklebank, C. C. N. Card and J. M. Smith, 'Low Reynolds number developing flows', *AIChE J.*, **15,** 548–553 (1969).
20. M. H. Wagner, 'Developing flow in circular conduits: transition from plug flow to tube flow', *J. Fluid Mech.*, **72,** 257–268 (1975).
21. L. Rosenhead, *Laminar Boundary Layers*, Dover, New York, 1988, pp. 144–150.
22. J. P. Johnston, 'Internal flows', in P. Bradshaw (ed.), *Turbulence; Topics in Applied Physics, Vol.* 12, 2nd edn, Springer, Berlin, 1978, pp. 109–169.